The Astrophysical Journal Letters, 896:L27 (7pp), 2020 June 20 https://doi.org/10.3847/2041-8213/ab97ac

Compact Radio Emission from Nearby Galaxies with Mid-infrared Nuclear Outbursts

B. B. Dai[1], X. W. Shu[1], N. Jiang[2], L. M. Dou[3], D. Z. Liu[4], C. W. Yang[5], F. B. Zhang[1], and T. G. Wang[2]
[1] Department of Physics, Anhui Normal University, Wuhu, Anhui, 241002, People's Republic of China; xwshu@mail.ahnu.edu.cn
[2] CAS Key Laboratory for Research in Galaxies and Cosmology, Department of Astronomy, University of Science and Technology of China, Hefei, Anhui 230026, People's Republic of China
[3] Center for Astrophysics, Guangzhou University, Guangzhou 510006, People's Republic of China
[4] Max Planck Institute for Astronomy, Königstuhl 17, D-69117 Heidelberg, Germany
[5] Polar Research Institute of China, 451 Jinqiao Road, Shanghai, 200136, People's Republic of China
Received 2020 March 5; revised 2020 May 19; accepted 2020 May 28; published 2020 June 16

Abstract

We present 5.5 GHz observations with the Very Large Array of a sample of nearby galaxies with energetic nuclear outbursts at mid-infrared (MIR) bands. These observations reach a uniform depth down to a median rms of $\sim$10 μJy, representing one of the most sensitive searches for radio emission associated with nuclear transients. We detect radio emission in 12 out of 16 galaxies at a level of $>5\sigma$, corresponding to a detection rate of 75%. Such a high detection is remarkably different from previous similar searches in stellar tidal disruption events. The radio emission is compact and not resolved for the majority of sources on scales of $\lesssim$0.″5 (<0.9 kpc at $z < 0.1$). We find that the possibility of the star formation contributing to the radio emission is low, but an active galactic nucleus (AGN) origin remains a plausible scenario, especially for sources that show evidence of AGN activity in their optical spectra. If the detections could represent radio emission associated with a nuclear transient phenomenon such as a jet or outflow, we could use the blast wave model by analogy with the gamma-ray burst afterglows to describe the evolution of radio light curves. In this context, the observations are consistent with a decelerating jet with an energy of $\sim 10^{51-52}$ erg viewed at 30°–60° off-axis at later times, suggesting that powerful jets may be ubiquitous among MIR-burst galaxies. Future continuous monitoring observations will be crucial to decipher the origin of radio emission through detections of potential flux and spectral evolution. Our results highlight the importance of radio observations to constrain the nature of nuclear MIR outbursts in galaxies.

Unified Astronomy Thesaurus concepts: Radio continuum emission (1340); Radio jets (1347); Dust continuum emission (412); Surveys (1671); Tidal disruption (1696); Active galaxies (17)

1. Introduction

It is generally accepted that super massive black holes (SMBH) reside at the cores of many galaxies (see the review by Graham 2015). When a star passes too close to an SMBH, it can be squeezed and torn apart once the tidal force of the SMBH exceeds the star's self-gravity (Stone et al. 2019). It is the so-called tidal disruption event (TDE), during which roughly half of the mass of the disrupted star falls back close to the event horizon of the black hole, generating a luminous flare of electromagnetic radiation (Rees 1988; Guillochon et al. 2014). As the stellar debris gets accreted effectively, a fraction of accretion power could be converted into outflow, leading to the formation of a relativistic jet, which can be detected at radio wavelengths (e.g., van Velzen et al. 2011b; Zauderer et al. 2011).

Over the past years, dozens of TDE candidates have been discovered at soft X-rays (Komossa 2015; Saxton et al. 2019) and ultraviolet wavelengths (UV; Gezari et al. 2009, 2012), and the number is expected to increase rapidly in the epoch of time-domain optical surveys (van Velzen et al. 2011a, 2020; Cenko et al. 2012; Arcavi et al. 2014). In contrast, radio follow-up observations of known TDEs have resulted in very few conclusive detections of jet emission (Bower et al. 2013; van Velzen et al. 2013). So far, very few jetted TDEs have been discovered with associated radio emission (Zauderer et al. 2011; Brown et al. 2017), including the prototypical source, Swift J1644+57, in which the radio emission is explained due to the interaction of the jet with the ambient medium (Giannios & Metzger 2011; Berger et al. 2012; Eftekhari et al. 2018). IGR J12580+0134 and Arp 299-B AT1 are found with a relativistic jet that is viewed off-axis (Irwin et al. 2015; Perlman et al. 2017; Mattila et al. 2018), and for the latter a resolved, expanding radio jet was directly imaged for the first time. The radio emission has also been detected from the thermal TDE ASASSN-14li (Alexander et al. 2016; van Velzen et al. 2016a) and XMMSL1 J0750-85 (Alexander et al. 2017), but with luminosities at least two orders of magnitude lower than Swift J1644+57, which can be explained by less energetic jets or nonrelativistic outflows. It is suggested that the outflows may be more ubiquitous than jets in TDEs (Alexander et al. 2016; Anderson et al. 2019), but most eluded detections due to insufficient sensitivity of radio observations. The current nondetections could also be explained by the delayed onset of the radio emission at early times. Yet the known TDEs with radio detections are still not enough to test these possibilities.

In a gas-rich circumnuclear environment, nuclear flares from TDEs can ionize and heat gas surrounding the black hole. When dust is present, the UV/optical photons are absorbed by dust and reemit in the infrared (IR). This dust emission is predicted to peak at 3–10 μm with an IR luminosity of 10^{42-43} erg s^{-1} and last for a few years for a typical TDE (Lu et al. 2016). Indeed, using archival data at 3.4 and 4.6 μm (W1 and W2 hereafter) from the WISE all-sky survey, such a dust reprocessed emission is detected in a few TDE candidates (Dou et al. 2016, 2017; Jiang et al. 2016; van Velzen et al. 2016b) providing a new opportunity in diagnosing the physical conditions of the circumnuclear material. Furthermore, the mid-infrared (MIR) dust echoes from nuclear transients are promising to reveal the population of dust-enshrouded TDEs

(Mattila et al. 2018), allowing for a more unbiased census of TDE phenomenon. In addition to TDEs, modern time-domain spectral observations have revealed a class of "changing-look" active galactic nuclei (CL AGNs), which can change their optical types on timescales of years, characterized by emerged or disappeared broad emission lines as well as dramatic continuum variations (e.g., Shappee et al. 2014; Gezari et al. 2017; Yan et al. 2019). More importantly, it has been proved that MIR variability is efficient in identifying candidates of CL AGNs (Sheng et al. 2017). The radio properties are crucial to understand the nature of CL AGNs, but are yet largely unexplored in observations.

In this Letter, we report the results from the radio observations of a sample of galaxies with nuclear MIR outbursts, revealing a high detection rate of 75% down to about 60 μJy ($\approx 5\sigma$). The observations and data reductions are described in Section 2. In Section 3, we present the properties of radio emission and discussions. In Section 4, we summarize our results and findings. We adopt a cosmology of $\Omega_{\rm M} = 0.3$, $\Omega_{\lambda} = 0.7$, and $H_0 = 70\,{\rm km\ s^{-1}\ Mpc^{-1}}$ when computing luminosity distance.

2. Observation and Data Reduction

Our sample of objects are selected from the on-going program to systematically identify MIR outbursts in nearby galaxies (MIRONG; N. Jiang et al. 2020, in preparation) from the WISE survey. We restricted the sample to include only sources not detected in the previous FIRST and NVSS survey, in order to reduce the possibility of radio-loud AGNs causing the transient IR emission. In addition, we require all objects to be nearby at $z < 0.1$. The final sample for Very Large Array (VLA) observations consists of 16 sources, with 9 being optically classified as star-forming or normal galaxies and 7 as AGNs based on the SDSS spectroscopy.[6] Note that we did not exclude the AGNs since recent works have suggested that the expected TDE rate in AGNs may be higher than the quiescent galaxies (e.g., Karas & Šubr 2007), and indeed the preexisting AGN activity is found present in a few TDE candidates (e.g., Blanchard et al. 2017; Shu et al. 2018; Liu et al. 2020). In addition, the inclusion of AGNs allows us to examine whether the radio detection rate is different as compared with normal galaxies.

All radio observations are performed with Jansky VLA in A configuration (program code: 18A-207) and at *C*-band with a total bandwidth of 2 GHz over the frequency range $4.5 \sim 6.5$ GHz, consisting of 16 subbands with 64 channels in each subband. We refer to the central frequency of 5.5 GHz in the following analysis. All observations are performed between 2018 March 9 and April 30, and each source has a total integration time of 25 minutes, with 10 minutes on-source and 15 minutes for calibrators. We selected the most suitable radio source close to target for amplitude and phase calibration, and 3C286 or 3C48 for bandpass and flux density calibration. The data were reduced following standard procedures with the CASA package. According to the pipeline log files, we examined each spectral window and flagged the abnormal data due to RFI or hardware issues. The calibrated data for each source were then selected and we used the CLEAN algorithm to remove possible contamination from side-lobes, with the conventional Briggs weighting and ROBUST parameter of 0. The final cleaned maps have a typical synthesized beam of $0\farcs3$–$0\farcs5$ and an rms noise of $\sim$5–20 μJy.

In addition to the new VLA *C*-band data, we also checked for the detectability of radio emission of the sample from the new VLA Sky Survey (VLASS) at *S*-band ($\approx$3 GHz), in which the quick-look imaging data are available.[7] The observations were performed between 2017 and 2019, with a median rms of 138 $\mu{\rm Jy\ beam^{-1}}$. We found that 3 out of 16 galaxies are detected at the *S*-band. In Table 1, we summarize the results of radio observations for the 16 sources. The columns represent (1) source name; (2) and (3) optical coordinate; (4) image rms near the source position, σ; (5) integrated flux density, in μJy; (6) peak flux density, in $\mu{\rm Jy\ beam^{-1}}$; (7) image beam size and position angle, in arcsecond and degree; (8) the host galaxy type as classified from the SDSS optical spectra;[8] (9) redshift z, and (10) optical [O III] line luminosity in ${\rm erg\,s^{-1}}$; (11) integrated flux density at *S*-band from the VLASS; (12) the time interval between the start of the IR flare and radio observations. For nondetections, we give a 3σ upper limit to the flux density, which is in the range $\sim$40–100 μJy.

3. Results and Discussions

As shown in Table 1, we detected radio emission in 12 out of 16 galaxies observed with VLA, with flux down to 60 μJy ($\approx 5\sigma$), i.e., a 75% detection rate. The detection rate in the subsample of AGNs ($\approx$86%) is slightly higher than that in galaxies ($\approx$67%). Figure 1 displays the WISE lightcurve, SDSS optical spectroscopy, and SDSS *r*-band image overlaid with radio contours for one star-forming galaxy and one AGN from the sample, respectively. We argue that the radio emission for the galaxy subsample may not be dominated by the AGN activity. We constructed a comparison sample from galaxies without MIR variability in the SDSS Stripe 82 region, where deep 1.4 GHz observations over 92 deg^2 were performed with VLA. The VLA survey has an angular resolution of $\approx 1\farcs8$ with a median rms noise of 52 $\mu{\rm Jy\ beam^{-1}}$, and is the deepest survey achievable to date over an area of $\sim$100 deg^2 (Smolčić et al. 2017). Assuming a typical radio spectral index of $\alpha = -0.7$ ($S_\nu \propto \nu^\alpha$, Smolčić et al. 2017), the sensitivity of the VLA Stripe 82 survey corresponds with an rms of $\sim$20 $\mu{\rm Jy\ beam^{-1}}$ at 5.5 GHz, comparable to our observations. To ensure similar host properties as our sample, the galaxies from Stripe 82 were matched to each source in redshift with $|\Delta z| \leqslant 0.005$ and WISE 22 μm magnitude with $|\Delta{\rm mag}| \leqslant 0.05$. We selected randomly five matched galaxies for each source, constituting a comparison sample with 80 galaxies in total. These galaxies were then cross-matched with the VLA Stripe82 catalog (Hodge et al. 2011), yielding only three radio detections, i.e., a detection rate of <5%. This indicates that the radio emission in our sample is possibly associated with the nuclear MIR bursts. Furthermore, we have compiled SDSS AGNs at $z < 0.1$ from the Stripe 82 survey, and matched them to the VLA data within the same area. We found radio detections in 61 out of 342 matched sources, i.e., 17.8% detection rate. Hence, the radio detection rate in our IR-burst galaxies seems to be higher than that of normal AGNs.

[6] One source in the sample, SDSS J1422+0609, is listed in the SDSS spectroscopy catalog and classified as a galaxy, but its spectrum has not been made public.

[7] https://archive-new.nrao.edu/vlass/quicklook/

[8] http://skyserver.sdss.org/dr16/en/tools/quicklook/summary.aspx?

Table 1
Radio Observation Results for the Sample of Galaxies with MIR Bursts

Name	R.A.	Decl.	Rms (μJy)	Integrated Flux (μJy)	Peak Flux (μJy beam^{-1})	Beam Size (PA)[a] (arcsec × arcsec(deg))	Host Type	Redshift (z)	log $L_{[\mathrm{O\ III}]}$ (erg s^{-1})	$F_{3\mathrm{GHz}}$ (μJy)	Δt (yr)
SDSS J1537+5814	234.2970	58.2389	5.8	673.1	667.7	0.32 × 0.25 (−14.28)	AGN	0.093	40.78	712	2.15
SDSS J1340+1842	205.1353	18.7051	11	<33	⋯	⋯	AGN	0.090	41.09	<414	3.79
SDSS J1422+0609[b]	215.7254	6.16483	11	205	205.7	0.30 × 0.28 (−3.86)	Galaxy	0.038	⋯	<417	2.70
SDSS J1133+6701	173.4830	67.0186	25	4544	4569	0.48 × 0.25 (86.77)	AGN	0.039	39.43	4050	3.83
SDSS J1549+3327	237.4799	33.4644	13	<39	⋯	⋯	Galaxy/SF	0.086	39.68	<330	2.74
SDSS J1357+4423	209.3621	44.3874	3.4	54.2	62.7	0.29 × 0.25 (−4.87)	Galaxy/SF	0.072	40.78	<546	4.26
SDSS J1328+6227	202.0482	62.4619	4.4	186.2	186	0.52 × 0.25 (−85.32)	AGN	0.092	41.34	<405	3.30
SDSS J1550+5330	237.6914	53.5092	12	1278	1279	0.52 × 0.25 (81.91)	Galaxy	0.066	40.87	748	4.54
SDSS J1632+4416	248.1951	44.2718	13	<39	⋯	⋯	Galaxy	0.058	39.23	<354	2.24
SDSS J1524+5314	231.1588	53.2496	10	204	192.3	0.31 × 0.25 (10.39)	Galaxy/SF	0.085	39.78	<318	3.29
SDSS J1657+2345	254.3617	23.7578	13	97	80.5	0.36 × 0.28 (86.51)	AGN	0.059	40.47	<366	2.66
SDSS J2217-0820	334.3995	−8.3450	5.1	135.3	131.9	0.38 × 0.27 (−20.88)	AGN	0.085	40.92	<480	3.35
SDSS J1217+0350	184.4094	3.84455	13	91	88.5	0.51 × 0.28 (−59.83)	Galaxy	0.073	40.33	<411	4.59
SDSS J1314+5116	198.7493	51.2725	8.6	91.2	88.1	0.31 × 0.25 (−34.12)	AGN	0.025	39.93	<339	3.93
SDSS J1156+3131[c]	179.1602	31.5200	32	<96	⋯	⋯	Galaxy/SF	0.080	40.94	<873	2.42
SDSS J1402+3922	210.5885	39.3700	4.5	117	107.1	0.38 × 0.26 (−84.11)	Galaxy/SF	0.064	40.70	<360	4.35

Notes.
[a] Beam size from the cleaned image.
[b] The source is in the SDSS spectroscopy catalog, but the spectrum is not available possibly due to fiber problems. We adopted its photometric redshift instead.
[c] The relatively large rms could be due to the contamination from a nearby brighter source.

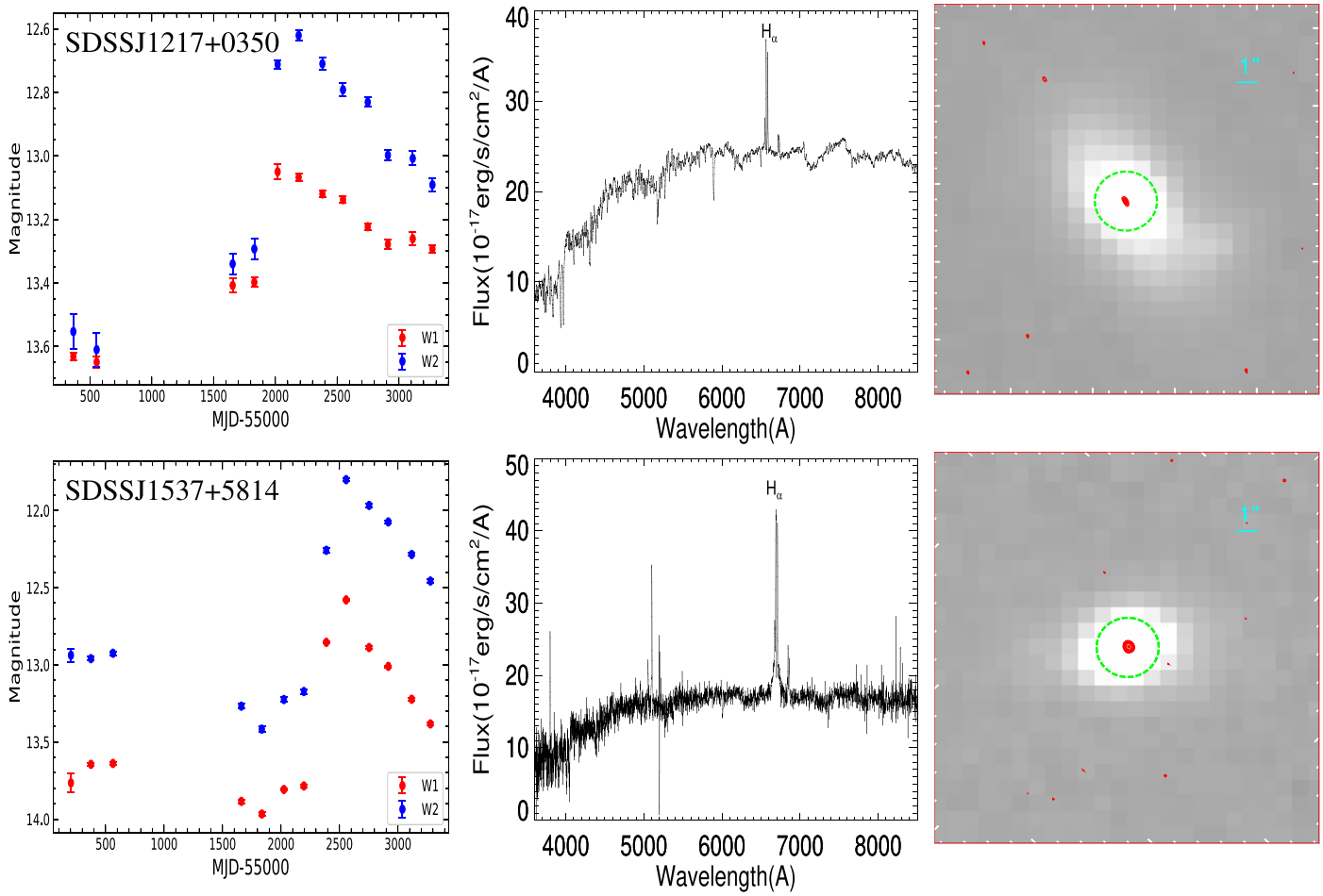

Figure 1. Multiwavelength characteristics of two typical sources in our sample, with one optically classified as a normal galaxy (top) and one as an AGN (bottom). From left to right, the WISE MIR light curve at W1 (red) and W2 (blue) bands, preflare SDSS optical spectrum of host galaxy, and SDSS *r*-band image overlaid with the VLA continuum contours (red). The green circle corresponds to the fiber size of SDSS spectroscopy, with a diameter of 3″. The image has a size of 18″ × 18″.

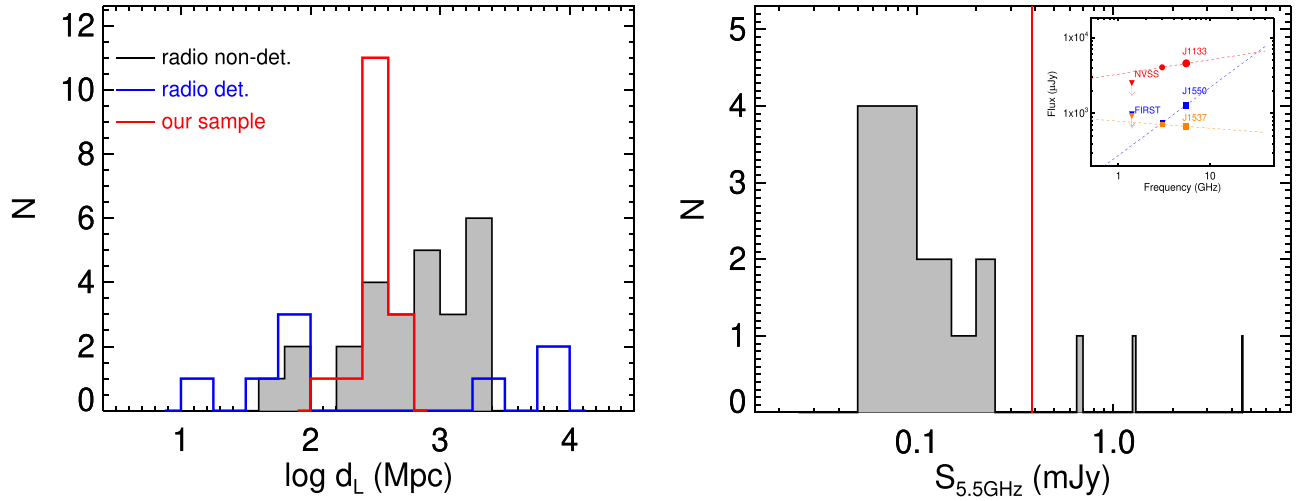

Figure 2. Left panel: luminosity distance (redshift) distribution as compared with the TDE sample with and without radio detections from the literature compilation (Berger et al. 2012; van Velzen et al. 2016a; Alexander et al. 2017; Blagorodnova et al. 2017; Brown et al. 2017; Perlman et al. 2017; Mattila et al. 2018; Anderson et al. 2019; Nicholl et al. 2019; van Velzen et al. 2019; Wevers et al. 2019; Gomez et al. 2020; Holoien et al. 2020). Right panel: distribution of flux densities as observed with VLA. The red vertical line represents the nominal 5σ upper limit of the FIRST survey converting to 5.5 GHz assuming a radio spectral index of $\alpha = -0.7$. The inset panel shows the radio flux and spectral slope for the three brightest sources in the sample, as compared with the FIRST/NVSS upper limits.

Most TDE candidates discovered in the optical and soft X-ray bands have no conclusive radio detections. van Velzen et al. (2013) performed a deep search for radio emission in seven thermal TDEs, and none of them are detected though the sensitivity of $\sim$10 μJy is comparable to ours. Bower et al. (2013) searched for the late time radio emission from seven

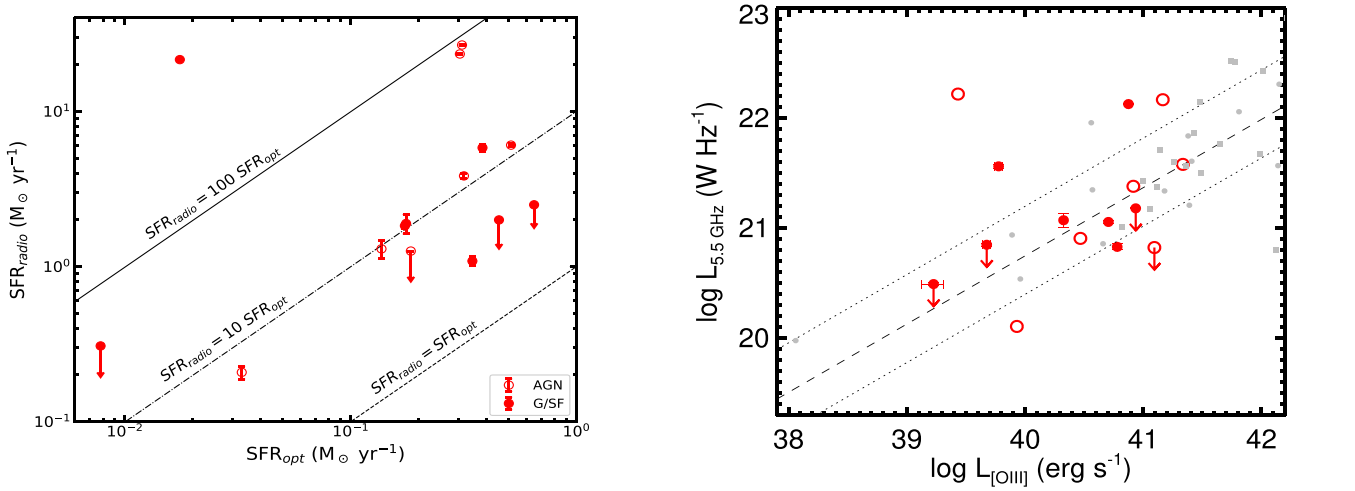

Figure 3. Left panel: comparison of radio-inferred SFRs with the SFRs obtained from SDSS fiber spectroscopy. The galaxy subsample is shown in solid circles, while the AGN subsample is shown in open circles. Right panel: radio luminosity vs. the extinction-corrected [O III]λ5007 luminosity. The dashed line represents the fit to radio-quiet Seyfert galaxies (Ho & Peng 2001).

X-ray selected TDE candidates and detected two with a flux level of $\sim$100 μJy. However, the radio identification for one source is ambiguous and the observed radio emission for another may be due to a highly variable AGN (van Velzen et al. 2016a). At a given sensitivity, the previous nondetections may result from a distance effect. In Figure 2 (left), we show the luminosity distance (converted from redshift) distribution of our sample, and the well-studied TDE candidates in the literature with and without radio detections for comparison. We found that except for jetted TDEs where the relativistic beaming effect is important, all previous radio-detected objects are within a redshift $z = 0.02$ (or $d_L \lesssim 90$ Mpc). Conversely, for the 26 TDE candidates without radio detections, only three at $z < 0.02$ and most at $z > 0.1$ with a median redshift of $z = 0.146$ ($d_L = 692$ Mpc). For comparison, all our sources at $z < 0.1$, with a median redshift of $z = 0.072$, seeming to fill the gap in redshift distribution between previous observations with and without radio detections. However, it should be noted that there is clear overlap between our sample and the TDEs that are not detected at radio. While the sensitivity is comparable to ours, we find half of them (those at $z < 0.1$) to have radio observations performed within 100 days since the optical discovery. In this case, the radio nondetections could be simply due to the delayed onset of jet/outflows at later times, which can be tested with future monitoring observations. Hence, we conclude that the distance effect can play a role, but is not enough to explain all radio nondetections.

The ratio of integrated flux to peak flux is in the range of 0.86–1.2, with a median value of 1.03, suggesting that most, if not all, radio emission is unresolved and extremely compact ($\lesssim$0.″5). We checked that the positional offsets of radio sources relative to the optical centers are in the range of 0.″03–0.″21, with a median offset of 0.″07, indicating that the radio emission originates from the nuclear region. The radio flux distribution is shown in Figure 2 (right). The median flux for the 12 detected sources is 186 ± 4.4 μJy, and the source with the brightest radio emission is SDSS J1133+6701 (J1133), which has an integrated flux density of $S_{5.5\ GHz} = 4.5 \pm 0.03$ mJy. In addition to J1133, two other sources in the sample, SDSS J1550+5330 (J1550) and SDSS 1537+5814 (J1537), have brighter radio flux and have also been detected by the VLASS at the *S*-band. Although the VLASS observations are not quasi-simultaneous (about a half year earlier) as ours, we attempted to measure the radio spectral index between the *S*-band and *C*-band for the three sources, as shown in Figure 2 (right, inset panel). We found that the radio slope is either flat or inverted, with α in the range of -0.09 to 0.89, suggesting the radio emission is from an optically thick region, likely in an early phase of evolution. More interestingly, using the spectral index, we extrapolated the VLA 5.5 GHz flux to 1.4 GHz for J1133, yielding a flux $S_{1.4\ GHz} = 3.5$ mJy, which is a factor of 1.4 higher than the 5σ upper limit of $S_{1.4\ GHz} = 2.5$ mJy beam^{-1} obtained from the NVSS survey. Considering the much larger beam size (by two orders of magnitude) of the NVSS survey, the expected flux difference is even larger. The results confirm that at least the radio emission for J1133 is transient (increased in flux).

Thanks to the high spatial resolution of the VLA observations, we have demonstrated that the radio emission is extremely compact as originating from the nuclear region. We begin to consider whether the detected radio emission could be due to a circumnuclear star formation process primarily from high-mass X-ray binaries and diffuse hot gas heated by supernovae. Under the assumption of star formation as the origin for the radio emission, we calculate the radio-inferred star formation rates (SFRs) based on the radio flux, using the expression given by (Greiner et al. 2016),

$$\mathrm{SFR_{radio}} = 0.059\ M_\odot \mathrm{yr}^{-1} \times F_{\nu,\mu\mathrm{Jy}} d_{L,\mathrm{Gpc}}^2 \nu_{\mathrm{GHz}}^{-\alpha} (1+z)^{-(\alpha+1)}, \quad (1)$$

where F_ν is the observed flux density at a frequency ν, and d_L is the luminosity distance at a source redshift. Since the expression is extrapolated from the relation between SFR and 1.4 GHz luminosity, we adopt a typical value of $\alpha = -0.7$ to account for proper *k*-corrections at 5.5 GHz. On the other hand, we cross-matched for each source with the SFRs as measured from the optical emission lines (mainly [O II]) within the 3″ given by the MPA-JHU SDSS spectroscopic catalog.[9] Figure 3 displays the comparison of radio-inferred SFRs with that obtained from optical emission lines. It can been seen that

[9] https://www.sdss.org/dr12/spectro/galaxy_mpajhu/

except for two objects, the radio-inferred SFRs are about an order of magnitude higher than the SDSS spectroscopic SFRs. Thus, we consider a star formation origin for the radio emission to be unlikely (with a contribution less than 10%). A single, young supernova seems also impossible to explain the observed radio emission, given the low SFRs in the nucleus for most of our sources ($\lesssim 0.3\,M_\odot\,\mathrm{yr}^{-1}$). In addition, the radio luminosities at 5.5 GHz are higher than the majority of the radio supernova remnant ($L_\nu \lesssim 10^{20}$ W Hz^{-1}) such as those studied in the starburst galaxy Arp 220 (Varenius et al. 2019).

Because of its compactness, the radio emission may be associated with persistent AGN activity or extreme AGN variability due to transient BH accretion, especially for sources that show evidence of an AGN from optical emission lines (∼50%). None of the sources are detected in the ROSAT survey, with an X-ray luminosity of $L_{0.2\text{–}2\ \mathrm{keV}} < 10^{41}\,\mathrm{erg\,s^{-1}}$, suggesting that they are either intrinsically weak or heavily obscured in the soft X-rays. It is suggested that optical [O III] λ5007 Å luminosity ($L_{[\mathrm{O\ III}]}$) is one of the best measures of the intrinsic luminosity of the nuclei of AGNs if present. Assuming all the power is due to AGNs, we show the relation between $L_{[\mathrm{O\ III}]}$ and radio luminosity in Figure 3 (right). The dashed line is the best fit to radio-quiet Seyfert galaxies from Ho & Peng (2001) for which the luminosities are plotted in gray dots. We also included the measurements from the radio-quiet narrow-line Seyfert 1 s (filled gray squares, Berton et al. 2016, 2018). The dotted line represents the approximately 1σ scatter at the luminosity range. While the majority of our sources (including upper limits) are consistent with the Ho & Peng (2001) relation within the 1σ scatter, there are four sources with more than 0.5 dex higher flux than expected. However, we note that since very few of the radio-quiet Seyferts from previous works have $L_{[\mathrm{O\ III}]} < 10^{41}\,\mathrm{erg\,s^{-1}}$ as the majority of our sources, the relation is very uncertain at low $L_{[\mathrm{O\ III}]}$. Based on the present data, we cannot rule out the weak-AGN origin for the radio emission. Actual detections of uniform radio flux variability are required to distinguish the origin from a transient accretion phenomenon or a weak persistent AGN.

We next consider whether the radio emission could be produced by a relativistic jet or outflow presumably due to the transient BH accretion, and its interaction with the circumnuclear medium (CNM). This is possible since our sample by selection is rich in dust and gas in the circumnuclear region. However, any initially relativistic jet (if present) would have decelerated to nonrelativistic velocities by the time of our radio observations. A similar process has been invoked in a gamma-ray burst (GRB) with external shocks from the decelerating blast wave potentially contributing to the radio emission. We attempted to place constraints on the presence of a relativistic jet by generating a grid of the GRB afterglow models with the BOXFIT code (van Eerten et al. 2012). Strictly speaking, the blast wave GRB jet model is not appropriate for AGN jets, so any conclusion should be treated with caution. In these models, the expansion of the jet in a uniform medium is calculated using relativistic hydrodynamical simulations. We assumed a CNM with constant density medium $n = 1\,\mathrm{cm^{-3}}$, a jet opening angle of $\theta_{\mathrm{jet}} = 0.1$, and the fraction of energy in the electrons and magnetic fields, $\epsilon_e = 0.1$ and $\epsilon_B = 0.01$, respectively. Then we used two intrinsic jet energies, $E_K = 10^{51}$, 10^{52} erg to generate light curves at different viewing angles. Light curves observed at 30°, 60°, and 90° from the jet axis are shown in Figure 4. For comparison, we also plot the observed light curve

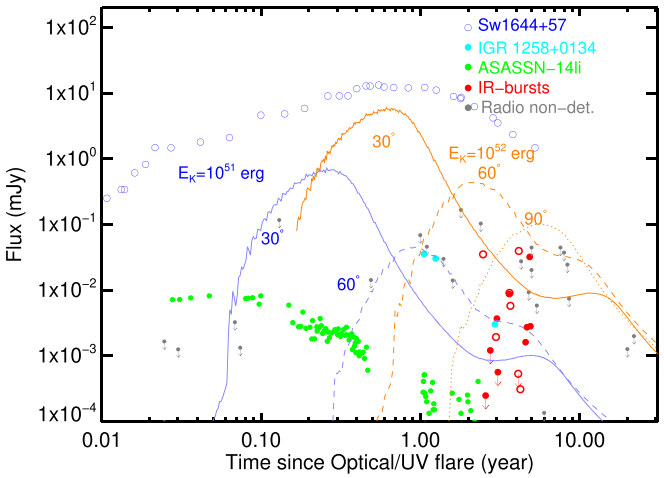

Figure 4. Radio flux is plotted with respect to the time of central optical/UV flare. For our sample, we assumed a typical distance of dust echo of 0.1 pc (van Velzen et al. 2016b) to estimate the approximate time of radio observations since central flare. The symbol has the same coding as in Figure 3. Radio light curve of the jetted TDE Sw 1644+57 (Berger et al. 2012; Eftekhari et al. 2018), the TDE IGR J12580+0134 with off-axis jet (Perlman et al. 2017), ASASSN14li with nonrelativistic outflow (Alexander et al. 2016; Bright et al. 2018), and upper limits for other optical/X-ray TDEs (gray dots, the same as shown in Figure 2, left) are also shown for comparison. All flux densities are scaled to the luminosity distance of Sw 1644+57. The orange and blue lines represent the blast wave model in analog with the GRB afterglow as calculated from the BOXFIT code (see the text).

of Sw J1644+57 with an on-axis relativistic jet, IGR J12580 +0134 with a jet viewed off-axis, and ASASSN-14li with a nonrelativistic outflow, respectively. Since our sample selection is based on the dust reprocessed emission, we assumed a typical dust echo distance of 0.1 pc (van Velzen et al. 2016b) to infer the time of radio observations with respect to the central optical/UV flare, which is around 2–5 yr. We find that, at least for the three sources with the brightest radio emission, a jet as powerful as Sw 1644+57 viewed at 30°–60° off-axis could yield consistent results with our observations. The radio emission for fainter sources could be consistent with the less energetic jet, similar to the off-axis jet observed in IGR J12580 +0134, though a nonrelativistic outflow is also possible if formed at a later time. Because the radio emission (if transient) is expected to continue declining in the next few years, multiepoch monitoring of these sources at radio bands is highly encouraged for comparison with models in detail.

On the other hand, comparing with the upper limits (5σ) of most optical/X-ray TDEs (gray dots), our late time radio observations are likely revealing that either the jet emission as powerful as J12580+0134 is ubiquitous among IR-selected outburst galaxies, or it is associated with a new weak-AGN variability mode. Future more sensitive late time radio observations of optical/X-ray TDEs will be helpful to test these possibilities. If the radio emission is due to TDEs, our radio observations of IR-selected flares have demonstrated that it is promising to reveal a new population of dust-obscured TDEs that are largely missed from previous optical surveys (Mattila et al. 2018). Studies on the multiwavelength properties of galaxies with nuclear IR-flares will be presented elsewhere.

4. Conclusion

We have presented VLA radio observations of galaxies with nuclear MIR outbursts that were discovered in the WISE all-

sky survey. We detect the radio emission at 5.5 GHz in 12 out of 16 galaxies down to the 5σ upper limit of $\sim$60 μJy, providing one of most sensitive searches for radio emission in nuclear transients such as TDEs. The majority of sources are unsolved at a resolution of $\lesssim$0.″5, indicating the radio emission is uniformly compact. The location of the radio emission is consistent with the optical center of the galaxy, with positional offsets less than 0.″2, supporting an origin from the nucleus. The SF contribution to the 5.5 GHz emission at a similar spatial scale is found to be low ($\lesssim$10%). The AGN origin for the radio emission remains a possible scenario with the current data. By checking for the VLASS data, we find radio detections in three sources and a flat or inverted radio spectrum between 3 GHz and 5.5 GHz for them, suggesting an origin from the optically thick region. We find convincing evidence in one source that the radio emission is transient. If explaining the radio emission as a jet interaction with the ambient medium, by analog with the blast wave model in GRB afterglows, we find the observations to be consistent with a decelerated jet viewed at 30°–60° off-axis, similar to the one observed in the TDE IGR J12580+0134. We have obtained follow-up observing time from the VLA for several sources in the sample, which will provide measurements of potential radio flux and spectral variability, and hence be able to shed new insight on the origin of the radio emission in galaxies with nuclear MIR outbursts.

The authors thank the VLA operations staff for their assistance in scheduling and performing the observations. We thank Hendrik van Eerten for kind advice on the use of the BOXFIT code. The National Radio Astronomy Observatory is a facility of the National Science Foundation operated under cooperative agreement by Associated Universities, Inc. This research made use of data products from the Wide-field Infrared Survey Explorer. The work is supported by Chinese NSF through grant Nos. 11822301, 11833007, U1731104, 11573001, and 11421303.

ORCID iDs

X. W. Shu https://orcid.org/0000-0002-7020-4290
N. Jiang https://orcid.org/0000-0002-7152-3621
L. M. Dou https://orcid.org/0000-0002-4757-8622
D. Z. Liu https://orcid.org/0000-0001-9773-7479
T. G. Wang https://orcid.org/0000-0002-1517-6792

References

Alexander, K. D., Berger, E., Guillochon, J., Zauderer, B. A., & Williams, P. K. G. 2016, ApJL, 819, L25
Alexander, K. D., Wieringa, M., Berger, E., Saxton, R., & Komossa, S. 2017, ApJ, 837, 153
Anderson, M., Mooley, K., Hallinan, G., et al. 2019, arXiv:1910.11912
Arcavi, I., Gal-Yam, A., Sullivan, M., et al. 2014, ApJ, 793, 38
Berger, E., Zauderer, A., Pooley, G., et al. 2012, ApJ, 748, 36
Berton, M., Congiu, E., Järvelä, E., et al. 2018, A&A, 614, A87
Berton, M., Foschini, L., Ciroi, S., et al. 2016, A&A, 591, A88
Blagorodnova, N., Gezari, S., Hung, T., et al. 2017, ApJ, 844, 46
Blanchard, P., Nicholl, M., Berger, E., et al. 2017, ApJ, 843, 106
Bower, G. C., Metzger, B. D., Cenko, S. B., Silverman, J. M., & Bloom, J. S. 2013, ApJ, 763, 84
Bright, J. S., Fender, R. P., Motta, S. E., et al. 2018, MNRAS, 475, 4011
Brown, G., Levan, A., Stanway, E., et al. 2017, MNRAS, 472, 4469
Cenko, S. B., Bloom, J. S., Kulkarni, S., et al. 2012, MNRAS, 420, 2684
Dou, L., Wang, T., Yan, L., et al. 2017, ApJL, 841, L8
Dou, L., Wang, T.-g., Jiang, N., et al. 2016, ApJ, 832, 188
Eftekhari, T., Berger, E., Zauderer, B., Margutti, R., & Alexander, K. 2018, ApJ, 854, 86
Gezari, S., Chornock, R., Rest, A., et al. 2012, Natur, 485, 217
Gezari, S., Heckman, T., Cenko, S. B., et al. 2009, ApJ, 698, 1367
Gezari, S., Hung, T., Cenko, S. B., et al. 2017, ApJ, 835, 144
Giannios, D., & Metzger, B. D. 2011, MNRAS, 416, 2102
Gomez, S., Nicholl, M., Short, P., et al. 2020, arXiv:2003.05469
Graham, A. W. 2015, ASSL, 418, 263
Greiner, J., Michałowski, M. J., Klose, S., et al. 2016, A&A, 593, A17
Guillochon, J., Manukian, H., & Ramirez-Ruiz, E. 2014, ApJ, 783, 23
Ho, L. C., & Peng, C. Y. 2001, ApJ, 555, 650
Hodge, J. A., Becker, R. H., White, R. L., et al. 2011, AJ, 142, 3
Holoien, T. W.-S., Auchettl, K., Tucker, M. A., et al. 2020, arXiv:2003.13693
Irwin, J. A., Henriksen, R. N., Krause, M., et al. 2015, ApJ, 809, 172
Jiang, N., Dou, L., Wang, T., et al. 2016, ApJL, 828, L14
Karas, V., & Šubr, L. 2007, A&A, 470, 11
Komossa, S. 2015, JHEAp, 7, 148
Liu, Z., Li, D., Liu, H.-Y., et al. 2020, ApJ, 894, 93
Lu, W., Kumar, P., & Evans, N. J. 2016, MNRAS, 458, 575
Mattila, S., Pérez-Torres, M., Efstathiou, A., et al. 2018, Sci, 361, 482
Nicholl, M., Blanchard, P. K., Berger, E., et al. 2019, MNRAS, 488, 1878
Perlman, E. S., Meyer, E. T., Wang, Q. D., et al. 2017, ApJ, 842, 126
Rees, M. J. 1988, Natur, 333, 523
Saxton, R., Motch, C., Komossa, S., et al. 2019, AN, 340, 351
Shappee, B. J., Prieto, J. L., Grupe, D., et al. 2014, ApJ, 788, 48
Sheng, Z., Wang, T., Jiang, N., et al. 2017, ApJL, 846, L7
Shu, X., Wang, S., Dou, L., et al. 2018, ApJ, 857, L16
Smolčić, V., Novak, M., Bondi, M., et al. 2017, A&A, 602, A1
Stone, N. C., Kesden, M., Cheng, R. M., et al. 2019, GReGr, 51, 30
van Eerten, H., van Der Horst, A., & MacFadyen, A. 2012, ApJ, 749, 44
van Velzen, S., Anderson, G. E., Stone, N. C., et al. 2016a, Sci, 351, 62
van Velzen, S., Farrar, G. R., Gezari, S., et al. 2011a, ApJ, 741, 73
van Velzen, S., Frail, D. A., Körding, E., & Falcke, H. 2013, A&A, 552, A5
van Velzen, S., Gezari, S., Cenko, S. B., et al. 2019, ApJ, 872, 198
van Velzen, S., Gezari, S., Hammerstein, E., et al. 2020, arXiv:2001.01409
van Velzen, S., Körding, E., & Falcke, H. 2011b, MNRAS, 417, L51
van Velzen, S., Mendez, A. J., Krolik, J. H., & Gorjian, V. 2016b, ApJ, 829, 19
Varenius, E., Conway, J., Batejat, F., et al. 2019, A&A, 623, A173
Wevers, T., Pasham, D. R., van Velzen, S., et al. 2019, MNRAS, 488, 4816
Yan, L., Wang, T., Jiang, N., et al. 2019, ApJ, 874, 44
Zauderer, B. A., Berger, E., Soderberg, A. M., et al. 2011, Natur, 476, 425